Nanoscale

PAPER

View Article Online
View Journal

Cite this: DOI: 10.1039/d4nr04169k

Low temperature multimode atomic force microscopy using an active MEMS cantilever†

Michael G. Ruppert, *[a] Miguel Wiche,[b] André Schirmeisen[b] and Daniel Ebeling *[b]

Received 9th October 2024,
Accepted 28th January 2025

DOI: 10.1039/d4nr04169k

rsc.li/nanoscale

High resolution atomic force microscopy is routinely performed at ultra-high vacuum and at low temperatures by employing a qPlus tuning fork sensor. Due to its intrinsic self-sensing capability, very high dynamic stiffness, and large *Q* factor, qPlus sensors are pre-dominantly used for obtaining atomic resolution. In this work, we present a proof of concept for an active microelectromechanical system (MEMS) microcantilever with integrated piezoelectric sensing and demonstrate its capability to obtain scanning tunneling microscopy as well as high-resolution non-contact atomic force microscopy images on an atomically flat Au(111) surface. Equipped with a focused ion beam deposited tungsten tip, the active MEMS cantilever is able to obtain high contrast scanning tunneling and frequency shift images at the fundamental and at a higher eigenmode of the cantilever.

Introduction

Low-temperature atomic force microscopy (AFM) under ultra-high vacuum (UHV) conditions is one of the most powerful tools in surface science. Further developments of the method, such as the functionalization of the AFM tip apex with a single carbon monoxide (CO) molecule, made it possible to achieve bond-level resolution and visualize the chemical structure of individual organic compounds.[1] This so-called bond imaging technique, has, for example, been applied to determine chemical structures of unknown compounds,[2–5] bond-orders,[6] intermediate states and products of chemical reactions,[7–11] three-dimensional absorption conformations,[12–14] self-assembly mechanisms,[15–19] vibrational properties,[20] electron spin transitions,[21] and absolute configurations of single aliphatic compounds by visual inspection.[22] Furthermore, the method can be utilized for constructing and characterizing covalent organic nanostructures one molecule at a time.[23]

The chemical bond imaging technique employs qPlus type quartz tuning fork sensors as state-of-the-art AFM probes.[24,25] A thin metal wire (usually tungsten or platinum/iridium) with a sharp tip glued to the end of the free prong serves as a local probe for simultaneously detecting the tip–sample forces and the tunneling current. The piezoelectric quartz material offers self-sensing capabilities, which is particularly suited for applications at low temperatures in UHV conditions since no laser is required for the signal read out. Furthermore, qPlus sensors provide stable operation with oscillation amplitudes in the regime of several picometers and high force sensitivity, which has led to their success in the field.

However, due to their relatively high spring constants (approx. 1800 N m^{-1}), qPlus sensors also require long averaging times and low measurement bandwidths to detect the minute tip–sample forces (in the range of several piconewtons). Typically, the sensors are operated in frequency modulation (FM) mode[26] using phase-locked-loop (PLL) electronics.[27] For achieving bond level resolution, frequency shifts on the order of a few Hz need to be detected. This requires measurement bandwidths on the order of some 10 Hz and scanning times per image frame on the order of some 10 minutes to hours. In addition, the low measurement bandwidth paired with the non-monotonic distance dependence of the frequency shift prohibits a robust tip–sample distance feedback.[14,28] This makes the investigation of three-dimensional molecules difficult.

The low experimental throughput of qPlus sensors can, for example, be addressed by using the *Q*-controlled amplitude modulation (AM) mode[28] while three-dimensional molecules become accessible using the tunneling current as a tip–sample feedback.[2,14,29,30] Another promising approach is the utilization of multifrequency imaging schemes where two or more

[a]University of Technology Sydney, Centre for Audio, Acoustics and Vibration, Ultimo, NSW 2007, Australia. E-mail: michael.ruppert@uts.edu.au
[b]Justus Liebig University Giessen, Institute of Applied Physics, Giessen, 35392, Germany. E-mail: daniel.ebeling@ap.physik.uni-giessen.de

† Electronic supplementary information (ESI) available: Details on the amplitude calibration of the first and third mode of the piezoelectric MEMS cantilever, LT-AFM/STM results at varying imaging speeds of the piezoelectric MEMS sensor and a qPlus sensor, as well as additional analysis on the effective signal-to-noise ratio for the STM and AFM frequency shift signals of the MEMS cantilever and qPlus sensor is provided in the supplementary material. See DOI: https://doi.org/10.1039/d4nr04169k

eigenmodes of the AFM sensor are simultaneously excited and measured.[31] It has been illustrated for applications in ambient conditions that each of the eigenmodes could serve for a different purpose, such as tracking the topography or high resolution compositional mapping.[32] Recently, it was shown that transferring such concepts to the bond imaging method with qPlus sensors allows higher flexural and torsional eigenmodes to be used to obtain lateral force microscopy images.[33,34] However, these studies also reveal the low detection sensitivity of qPlus sensors at those higher eigenmodes as well as imaging artifacts resulting from subtle lateral tip vibrations.[34,35]

In this article, we present a proof of concept for a piezoelectric MEMS-based cantilever with an integrated tungsten tip that can, as an alternative to conventional qPlus sensors, address such drawbacks. MEMS-based cantilevers were already used in ambient conditions for multifrequency AFM,[36] off-resonance AFM,[37] to avoid optical beam deflection in light sensitive environments,[38,39] or to increase the experimental throughput by employing cantilever arrays.[40] Here, we demonstrate experimentally that the piezoelectric MEMS cantilever can achieve comparable imaging contrast in the frequency shift signal while performing simultaneous low-temperature scanning tunneling microscopy and atomic force microscopy. This highlights the potential of this approach for imaging applications which require a minimal thermal footprint as well as integrated actuation and sensing capability.

Results

Cantilever design

The piezoelectric MEMS cantilever design is shown in Fig. 1(a) and consists of a stepped rectangular cantilever geometry leading to closely spaced higher eigenmodes.[41] This design is chosen such that higher eigenmodes of the sensor still fall within the measurement bandwidth of the preamplifier of the LT-AFM system. Detailed mechanical modeling of such MEMS cantilevers with stepped geometry can be found in ref. 42. The cantilever consists of a base section with dimensions of 600 μm × 400 μm and a tip section with dimensions of 400 μm × 112 μm. The piezoelectric transducers are symmetrically arranged on the base section of the cantilever and are individually routed to wirebonding pads located on the cantilever chip. The center piezoelectric transducer is additionally guarded with a ground trace to facilitate integrated actuation and sensing with minimal electrical feedthrough.[43] In this

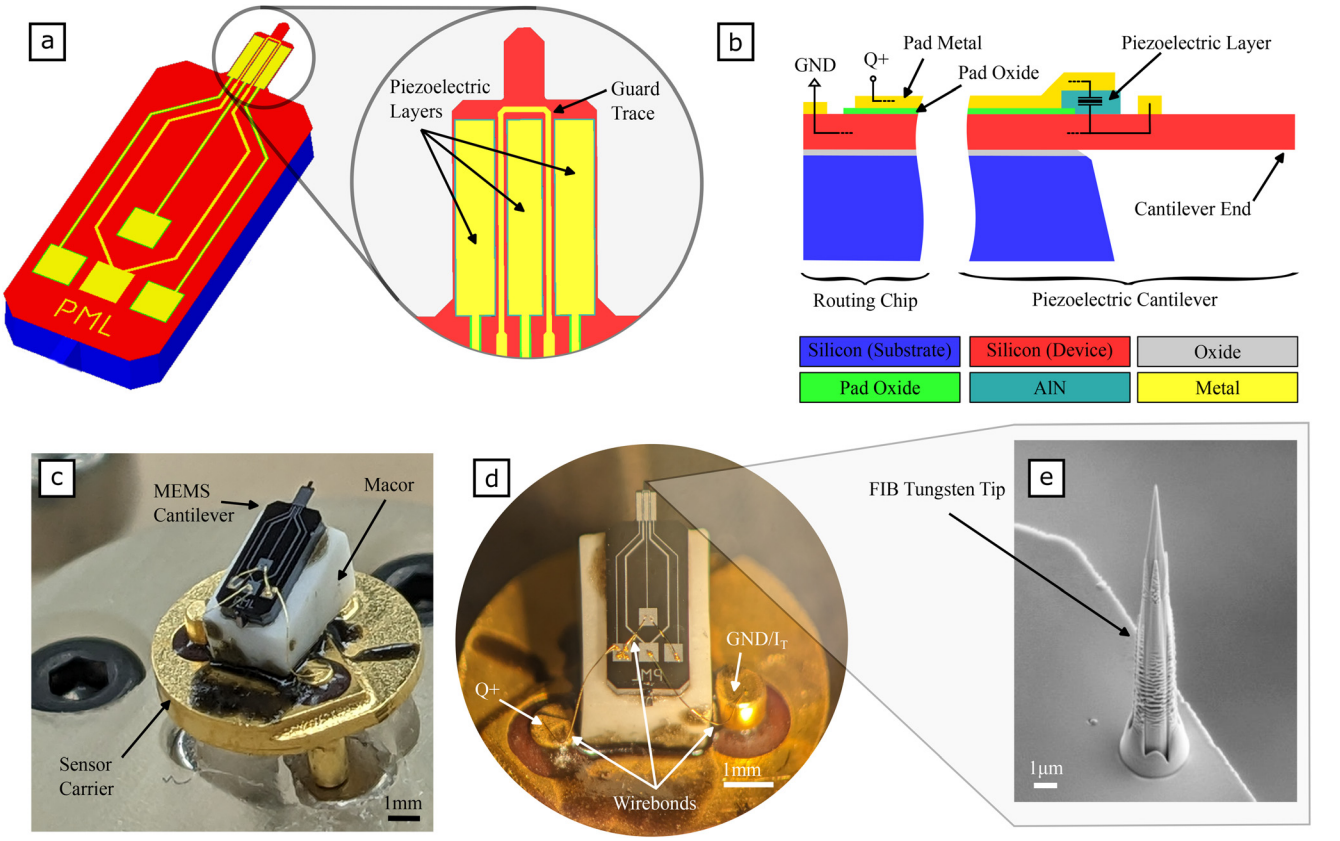

Fig. 1 (a) Schematic top view of the piezoelectric MEMS cantilever design. (b) Cross-section view of the piezoelectric MEMS cantilever and layer stack-up. (c) and (d) Photos of the fabricated MEMS cantilever wire-bonded to a qPlus gold sensor carrier. (e) Scanning electron micrograph of the focused ion beam deposited tungsten tip.

work, all piezoelectric transducers are wirebonded together since only the sensing functionality is employed.

The dimensions were chosen such that the fundamental resonance frequency is close to the fundamental resonance frequency of commonly used qPlus sensors.[25,35] This was confirmed *via* finite element analyses using CoventorWare for which the 5-mask PiezoMUMPS® fabrication process[44] has been modeled. Using modal analysis, the fundamental resonance frequency is found to be f_1 = 27.34 kHz with a modal stiffness of k_1 = 41.69 N m^{-1}. The resonance frequencies and modal stiffnesses of the first three flexural modes are summarized in Table 1.

The piezoelectric MEMS cantilever was fabricated with the rapid multi-user MEMS prototyping process PiezoMUMPS® (MEMSCAP Inc.),[44] a commercial micro fabrication service now provided by the Science Foundry. A schematic cross-section view of the layer stack is shown in Fig. 1(b). The PiezoMUMPS® process is based on a n-type (100) oriented silicon-on-insulator (SOI) wafer with a 400 μm ± 5 μm substrate thickness, oxide thickness of 1 μm ± 0.05 μm and a device layer of single-crystal-silicon with a thickness of 10 μm ± 1 μm. The top surface of the device layer is doped by depositing a phosphosilicate glass layer and annealing in Argon and is therefore highly conductive, serving as the ground return path for the piezoelectric sensing layers. The resistivity of the device layer was measured at 4.9 ± 0.1 mΩ cm,[45] however information on doping concentration and depth is not available from the manufacturer. To form piezoelectric sensor regions, a 0.5 μm layer of piezoelectric aluminum-nitrate (AlN) with a piezoelectric strain coefficient $d_{33} \approx$ 3.4–6.5 pC N^{-1} is used and a metal layer stack of 20 nm chrome and 1 μm aluminum is employed to provide electrical connections. Finally, a 20 nm thick thermal oxide layer provides electrical isolation between the device layer and the AlN and metal layers.

Sensor fabrication

A custom sensor carrier was equipped with a macro substrate to which the MEMS cantilever is glued using conductive EPO-TEK E2101. The bonding pads of the MEMS cantilever were subsequently wire-bonded to the gold studs of the sensor carrier where all the piezoelectric regions were connected to the Q^+ pin and the ground return is connected to the I_T pin. Photos of the fabricated device wire-bonded to the qPlus sensor carrier are shown in Fig. 1(c) and (d).

Direct focused ion beam (FIB) deposition of tungsten using a FEI Helios Nanolab G3 CX DualBeam FIB/SEM was used to form a multi-segment tip which is subsequently sharpened using tilted FIB milling.[36] A scanning electron micrograph image of the tip is shown in the inset in Fig. 1(e). The diameter of the tip base is approximately 3 μm and the height is approximately 12 μm. The tungsten tip is grounded *via* the direct connection to the device layer. In this setup, the STM gap voltage can be applied to the sample and the tunneling current is measured on the sample side.

Table 1 Cantilever modal parameters obtained from finite element analysis

Mode	Frequency [kHz]	Stiffness [N m^{-1}]
Mode 1	27.34	41.69
Mode 2	140.8	335.5
Mode 3	301.0	1279

Ambient results

The sensor was tested in ambient conditions with a laser Doppler vibrometer (Polytec, MSA-100-3D) using the measurement setup shown in Fig. 2(a); a photo of the experimental setup is shown in Fig. 2(b). Here, the MEMS cantilever was excited with a periodic chirp signal using direct electrical excitation of the piezoelectric layers *via* the Q^+ pin and the resulting mechanical response of the sensor is measured optically and plotted in Fig. 2(c). Also shown in the insets of Fig. 2(c) are the normalized experimentally measured deflection mode shape scans at the respective resonance frequencies. While the cantilever is undergoing harmonic motion due to excitation at one of its resonance frequencies, any deflection at the tip is measured by the piezoelectric sensors located near the base, which is the location of maximum strain.[37,42] Note that two different sensors from the same wafer were used for the measurements in ambient conditions and inside the LT-AFM. The differences can be seen in slightly varying resonance frequencies (sensor 1 (ambient results): f_1 = 29.53 kHz, sensor 2 (low temperature results): f_1 = 29.84 kHz).

The modal stiffnesses of the first three modes of the piezoelectric MEMS cantilever are experimentally determined using the thermal noise method.[46] For this purpose, the piezoelectric layers and all pins of the sensor carrier are grounded and the velocity power spectrum at the end of the cantilever is measured using a laser Doppler vibrometer (Polytec, MSA-100-3D). The thermal stiffness at each mode is obtained by performing a Lorentzian function fit to the measured thermal noise response.[47,48] The resulting spectra and the corresponding Lorentzian function fits are shown in Fig. 2(d). The experimentally determined modal stiffnesses of the first three flexural modes are summarized in Table 2 and match the simulated stiffnesses in Table 1 within acceptable tolerances. Deviations are associated with the laser location during the experimental thermal noise measurement, the absence of the tip in the simulation results, and uncertainties associated with the piezoelectric coefficient d_{31}. The noise floor of the laser Doppler vibrometer is around 30 fm $\sqrt{\text{Hz}}^{-1}$.

Low-temperature results

The piezoelectric MEMS cantilever was integrated with a commercial low-temperature atomic force microscope/scanning tunneling microscope (Scienta Omicron, LT-AFM/STM) at ultra-high vacuum ($p < 1 \times 10^{-10}$ mbar) and low temperature ($T \approx$ 5.2 K). An external phase-locked loop (PLL) (Zurich Instruments, MFLI) was used to operate the cantilever with a constant amplitude in frequency modulation mode. Unless otherwise stated, the PLL and amplitude controller bandwidth

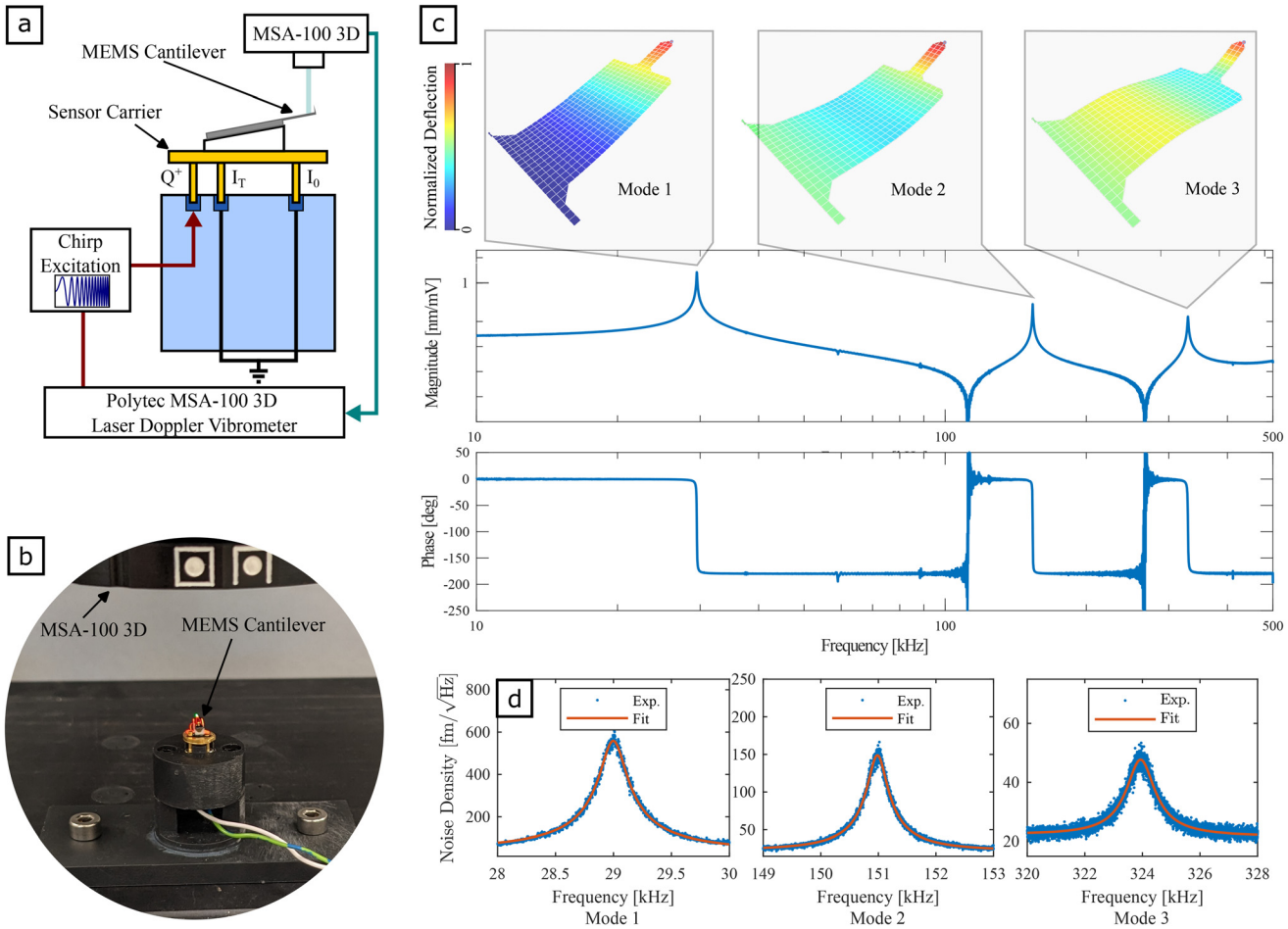

Fig. 2 (a) Schematic and (b) photo of the experimental setup for measuring the frequency response, mode shape scans, and thermal noise response with a Polytec MSA100 laser Doppler vibrometer in ambient conditions. (c) Frequency response for the first three modes of the piezoelectric MEMS cantilever measured with the setup shown in (a) and (b); the insets show the experimentally measured deflection mode shape scans at the respective resonance frequencies. (d) Thermal noise response and Lorentzian function fit of the first three modes of the piezoelectric MEMS cantilever measured with the setup shown in (a) and (b) with all electrodes grounded.

Table 2 Cantilever modal parameters from experimental analysis in ambient conditions

Mode	Frequency [kHz]	Stiffness [N m^{-1}]	Q-factor
Mode 1	29.53	35.07	395.4
Mode 2	153.7	333.9	601.6
Mode 3	329.6	1412	328.5

was set to 50 Hz. Combined STM/AFM imaging is performed by measuring the frequency shift signal from the MEMS cantilever while employing simultaneous tunneling current feedback.[14] All STM and AFM imaging results presented consist of the raw data, no post-processing was applied. A clean Au(111) surface was used for the experiments; the Au(111) single crystal (MaTeck) was prepared in the UHV system by several sputtering and annealing cycles.

The tungsten tip of the piezoelectric MEMS cantilever sensor was first sharpened in the LT-AFM/STM by voltage pulses between −8 V to +8 V and indentations into the Au(111) surface up to 1.8 nm. The tip conditioning was repeated until good image contrast and stable imaging could be achieved. While it was noted that voltage pulses lead to abrasion of tip material, it was not clear whether this is due to tip contamination or due to the more delicate tip integrity. A closer investigation of the limitations of FIB deposited tungsten tips in comparison to conventional tungsten wires glued to the prong of qPlus sensors is the scope of future research.

The frequency response at the first and third mode of the piezoelectric MEMS cantilever were measured inside the LT-AFM at 5.2 K by mechanically exciting the sensor and measuring the resulting deflections with the instrument's integrated low-temperature current amplifier connected to the piezoelectric layers *via* the Q^+ pin. The resulting responses are shown in Fig. 3(a) and (b). Within a narrow bandwidth around the resonances, a Lorentzian function fit is used to extract the quality factor which was recorded at 32 168 at the first mode (f_1 = 29.8414 kHz) and 26 571 at the third mode (f_3 = 331.8186

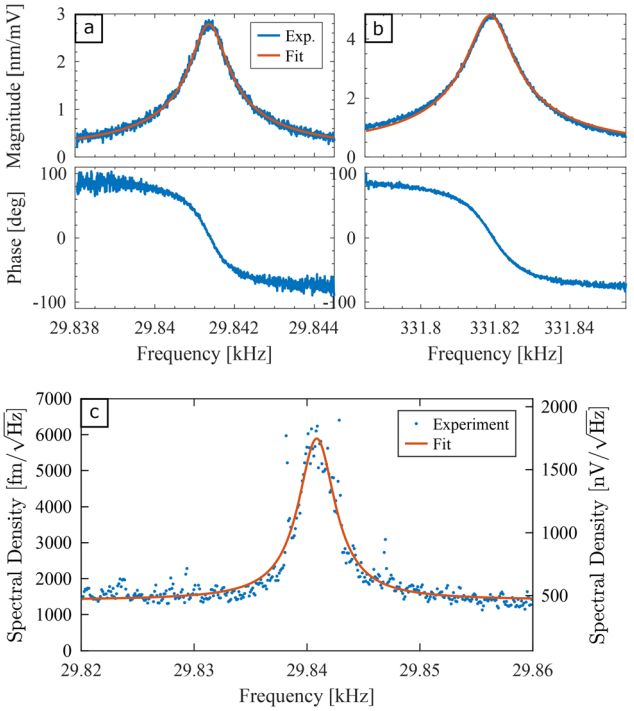

Fig. 3 Frequency response of (a) the first mode and (b) the third mode of the piezoelectric MEMS cantilever measured inside the LT-AFM, a Lorentzian function fit is used to extract the *Q* factor. (c) Thermal noise response and Lorentzian function fit at the first mode of the piezoelectric MEMS cantilever measured inside the LT-AFM.

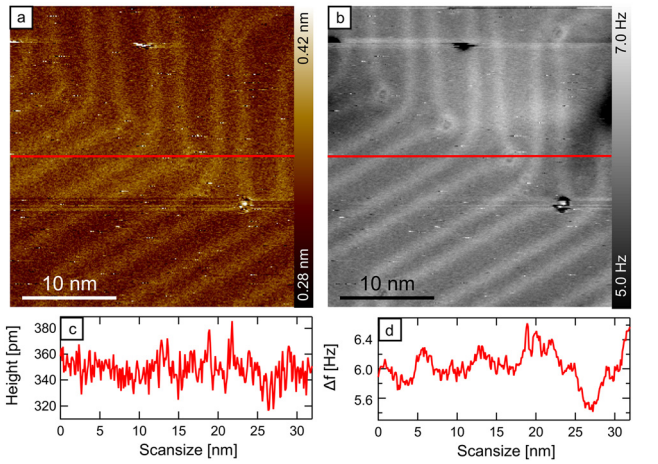

Fig. 4 High-resolution LT-AFM/STM images obtained with the first mode of the piezoelectric MEMS cantilever of the Au(111) herringbone reconstruction showing (a) STM image, (b) frequency-shift image, (c) cross-section of (a), and (d) cross-section of (b). Imaging conditions: I_t = 30 pA, V = 100 mV, image size = 30 × 30 nm, 300 × 300 pixel, raster time = 8 ms per pixel, scan speed = 12.5 nm s^{-1}, A_0 = 3.1 nm.

kHz). It was found that quality factor measurements are strongly influenced by the mechanical and electrical connection between the sensor carrier and carrier holder inside the LT-AFM/STM. This is, however, related to the design of the 3-pin sensor carrier and also observed with qPlus sensors. Due to the layout of the piezoelectric layers on the MEMS cantilever, the second mode is not observable due to charge cancellation.[36]

A thermal noise spectrum was also recorded using the ZoomFFT function of the external lock-in amplifier (Zurich Instruments, MFLI) around a narrow bandwidth around the first mode and is shown in Fig. 3(c). The noise floor off resonance is around 467 nV $\sqrt{\text{Hz}}^{-1}$ in the voltage domain. The deflection sensitivity was determined by systematically stepping the oscillation amplitude and recording the tunneling feedback controller output in constant current mode[49] (see Fig. S1 and S2 in ESI†). This procedure yields a sensitivity of 3.09 nm mV^{-1} on the first mode and leads to a noise floor off resonance of around 1441 fm $\sqrt{\text{Hz}}^{-1}$ in the displacement domain. The deflection sensitivity on the third mode was determined to be 4.33 nm mV^{-1} using the same procedure as for the first mode.

AFM/STM at mode 1 of the MEMS cantilever. Combined STM/AFM imaging with the first mode of the piezoelectric MEMS cantilever is demonstrated in Fig. 4. Despite the relatively large amplitude of the cantilever of 3.1 nm, the frequency shift image in Fig. 4(b) has a much better contrast than the STM image in Fig. 4(a) and clearly reveals atomic defects in the elbow region of the Au(111) herringbone reconstruction. This is also evident from comparing the scan lines in Fig. 4(c) with Fig. 4(d).

AFM/STM at mode 3 of the MEMS cantilever. A major benefit of employing active microcantilever type sensors for AFM is their ability to explore higher eigenmodes which is of high interest for the application of multifrequency imaging modes.[34] Due to the stepped geometry of the piezoelectric MEMS cantilever in this work, the resonance frequency of the third mode still falls within the bandwidth of the integrated AFM current preamplifier (which is designed for detecting the fundamental eigenmode of qPlus sensors).

A high-resolution STM/AFM image on the third mode of the piezoelectric MEMS cantilever at a raster time of 30 ms per pixel is shown in Fig. 5. Excellent image contrast in both the STM and frequency shift channel is observed, clearly highlighting the atomic defects in the elbow region of the Au(111) herringbone reconstruction. Typical adsorbates such as CO molecules or impurities from the metal crystal are likely located at the elbow regions due to their relatively high reactivity. The different appearance of the atomic defect features in Fig. 5(a) and (b) is probably due to a different type or number of adsorbates. As the four atomic defect features in the lower right of Fig. 5 are each showing two bright protrusions in the STM topography, it is assumed that they are made up of two adsorbates each.

Comparison with conventional qPlus sensors. In the ESI in Fig. S3,† we show a series of STM/AFM images taken with the third mode of the piezoelectric MEMS cantilever and an amplitude of 1.08 nm at five different scanning speeds ranging from 6.25 to 100 nm s^{-1}. The Au(111) herringbone reconstruction as

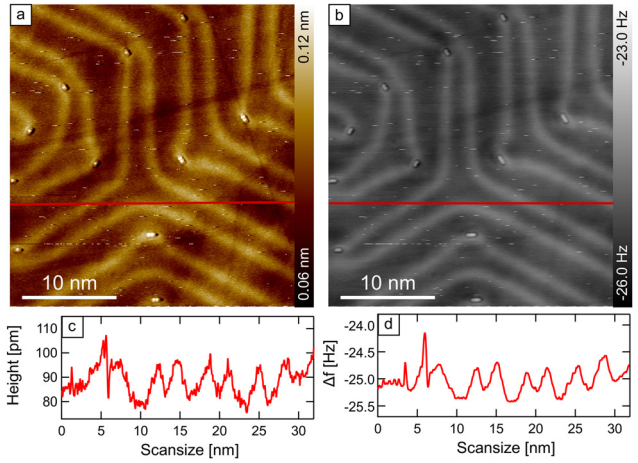

Fig. 5 High-resolution LT-AFM/STM images obtained with the third mode of the piezoelectric MEMS cantilever of the Au(111) herringbone reconstruction showing (a) STM image, (b) frequency-shift image, (c) cross-section of (a), and (d) cross-section of (b). Imaging conditions: I_t = 50 pA, V = 100 mV, image size = 30 × 30 nm, 600 × 600 pixel, raster time = 30 ms per pixel, scan speed = 1.67 nm s^{-1}, A_0 = 1.08 nm. The PLL bandwidth was set to 1 Hz.

well as atomic size defects are revealed in the STM topography at all tested imaging speeds. Frequency shift images clearly identify the Au(111) herringbone reconstruction, even for high imaging speeds of 100 nm s^{-1} (Fig. S3(f)†) and atomic defects are resolved at an imaging speed of 50 nm s^{-1} (Fig. S3(g)†) and slower.

For comparison, these measurements were also performed with a qPlus sensor at the same imaging parameters (see Fig. S4 and S5 in the ESI†). Here, an oscillation amplitude of 50 pm was chosen, a value typically used for bond imaging measurements. The STM topography images reveal a higher contrast and stability in case of the qPlus sensor. However, for the frequency shift channel, we find that the contrast of the herringbone reconstruction is rather weak for low scanning speeds (Fig. S4(i) and (j)†) and for speeds ≥25 nm s^{-1}, the reconstruction is no longer recognizable.

To objectively quantify the imaging performance, we determined the effective signal-to-noise ratio (SNR) of the images with a method introduced in ref. 28. Therefore, we separate the image noise from the signal by 2D FFT filtering and dividing the two components (see ESI Fig. S6 and Fig. S7† for details). Our analysis reveals an overall three to four times higher effective SNR for the qPlus sensor in case of STM topography images. For AFM frequency shift images, there is strong dependency on the imaging speed. At a rather low imaging speed of 1.67 nm s^{-1}, the effective SNR of the qPlus sensor is around 1.4 times higher than for the MEMS sensor (see Table S1 in ESI†). However, for a scan speed of 25 nm s^{-1}, the effective SNR of the MEMS device is 1.3 times higher than for the qPlus sensor. We attribute this to the overall higher absolute frequency shifts that are obtained with the MEMS sensor. Please note that this was even achieved with an amplitude of the MEMS sensor of ≈ 1 nm, which was approximately 20 times higher than the amplitude of the qPlus sensor.

Discussion

Compared to qPlus sensors, which are conventionally used for high-resolution atomic force microscopy under UHV conditions and at low temperatures, the MEMS-based cantilever sensor presented in this work has a more than 50-times lower stiffness on the first mode (qPlus sensors usually show a stiffness of 1800 N m^{-1} on the first mode[25]). As a result, significantly higher oscillations amplitudes (around 3 nm on the first mode and around 1 nm on the third mode) had to be employed to avoid snap-to-contact and imaging instabilities. Both eigenmodes of the piezoelectric MEMS cantilever investigated in this work show very high quality factors of around 25 000–30 000, comparable with those obtained with qPlus sensors. As a result, we are able to clearly demonstrate the ability to image atomically flat surfaces with single atomic defects of the Au(111) herringbone reconstruction in both, the tunneling current and the frequency shift channel. We also demonstrate the use of a post-fabricated focused ion beam deposited tungsten tip for low temperature STM and AFM measurements. While we observed material abrasion during tip conditioning experiments (voltage pulses and sample indentations), the initial results presented in this work show great promise for such tips.

The benefit of such MEMS cantilevers over conventional qPlus sensors is that their parameters, such as their dimensions and geometry, spring constant and resonant frequency can be tuned in wide ranges.[48,50] As a result, it can be seen that by decreasing the spring constant, higher frequency shifts and therefore a higher measurement bandwidth can be attained. With the added flexibility of determining the integrated piezoelectric sensor locations at the design level, we also demonstrate that higher flexural eigenmodes are accessible and can be used to obtain high resolution STM/AFM images.

Fabrication of such piezoelectric MEMS cantilevers may be challenging requiring access to complex microfabrication facilities. However, we have demonstrated that the commercial multi-user microfabrication service PiezoMUMPS® (MEMSCAP Inc., now Science Foundry)[44] can achieve excellent results if used in combination with post-fabricated FIB tungsten tips. Currently, this process is limited to employing aluminum nitride (AlN) as the piezoelectric layer which has a low to moderate piezoelectric coefficient (d_{33} ≈ 3.4–6.5 pC N^{-1}), comparable with those obtained for quartz based qPlus sensors.[25] To improve performance, new piezoelectric material deposition capabilities such as Scandium-doped AlN (ScAlN)[51] have recently emerged and demonstrated to provide a significant increase of the piezoelectric coefficient.

Currently, the deflection noise density of the proposed piezoelectric MEMS cantilever is higher than the best reported values in literature for qPlus sensors[52] which is associated

with the moderate to low piezoelectric coefficient of aluminum nitride (AlN) and lower stiffness of the sensor leading to a moderate to low deflection sensitivity. Additionally, a higher piezoelectric capacitance and non-optimized read-out electronics contribute to an overall higher noise floor in the voltage domain.[36] Since the frequency shift sensitivity is a function of the stiffness, resonance frequency, and oscillation amplitude of the sensor,[25] finding an optimal trade-off between these parameters will be investigated in future work.

Conclusion

This work demonstrates a first proof of concept study for the applicability of MEMS-based active microcantilever sensors for ultra-high vacuum and low-temperature scanning tunneling microscopy and atomic force microscopy. At this stage, the observed effective SNR of the tested MEMS device is around three to four times lower in case of STM topography images. However, for AFM frequency shift images, the performance of the MEMS device is comparable to qPlus sensors at low imaging speeds and around 1.3 times better than qPlus sensors at high imaging speeds.

Compared to conventionally used qPlus sensors, MEMS-based cantilever sensors with active piezoelectric sensing regions offer several interesting features. These include the ability to influence the sensor stiffness by direct design of the cantilever geometry, the ability to easily switch between higher modes of the cantilever and the ease of up-scaling the fabrication process. This opens up a number of opportunities for improvement of the presented results, for instance, finding the optimal cantilever stiffness which is a trade-off between allowing small oscillation amplitudes (favoring a higher dynamic stiffness) and maximizing the sensitivity in the frequency shift channel (favoring a lower dynamic stiffness). In subsequent work, the authors also aim to improve the noise performance of the presented sensor, both in terms of piezoelectric deflection sensitivity due to geometrical and material properties, but also in terms of the electrical read-out configuration. Finally, qPlus sensors still mostly rely on external piezo-acoustic excitation which renders the identification and use of higher order eigenmodes difficult, sometimes impossible. While third and fourth generation qPlus sensors feature additional electrodes for direct excitation,[25] the design of these electrodes is still intended for reading the fundamental eigenmode, which might lead to lower performance when using certain higher eigenmodes.[33–35] In contrast, MEMS-based sensors offer the ability to include dedicated piezoelectric actuation layers (in this work, these have been all connected to form a single sensing region) whose location and shape can be determined to maximize sensitivity at multiple higher eigenmodes.[42] Not only would this allow pre-calibration of the deflection sensitivity, but it would also lead to clean frequency responses such as shown in Fig. 2(c) to be obtained inside the LT-AFM.

Data availability

All relevant data are displayed within the manuscript and its ESI.†

Conflicts of interest

There are no conflicts of interest to declare.

Acknowledgements

M. G. R. is the recipient of an Australian Research Council Discovery Early Career Award (DE240100507) funded by the Australian Government. M. G. R. and D. E. wish to acknowledge the funding support from the German Research Foundation (Deutsche Forschungsgemeinschaft, DFG) under the category 'Initiation of International Collaborations' with reference EB 535/2-1. Further funding was provided by the Deutsche Forschungsgemeinschaft *via* grants EB 535/1-1, EB 535/4-1 and the Research Training Group "Substitute Materials for sustainable Energy Technologies, RTG-2204" as well as the LOEWE Program of Excellence of the Federal State of Hesse *via* the LOEWE Focus Group PriOSS 'Principles of On-Surface Synthesis'.

References

1 L. Gross, F. Mohn, N. Moll, P. Liljeroth and G. Meyer, The Chemical Structure of a Molecule Resolved by Atomic Force Microscopy, *Science*, 2009, **325**, 1110.
2 L. Gross, F. Mohn, N. Moll, G. Meyer, R. Ebel, W. M. Abdel-Mageed and M. Jaspars, Organic structure determination using atomic-resolution scanning probe microscopy, *Nat. Chem.*, 2010, **2**, 821.
3 K. Hanssen, *et al.*, A Combined Atomic Force Microscopy and Computational Approach for the Structural Elucidation of Breitfussin A and B: Highly Modified Halogenated Dipeptides from Thuiaria breitfussi, *Angew. Chem., Int. Ed.*, 2012, **51**, 12238.
4 Q. Fan, D. Martin-Jimenez, D. Ebeling, C. K. Krug, L. Brechmann, C. Kohlmeyer, G. Hilt, W. Hieringer, A. Schirmeisen and J. M. Gottfried, Nanoribbons with Nonalternant Topology from Fusion of Polyazulene: Carbon Allotropes beyond Graphene, *J. Am. Chem. Soc.*, 2019, **141**, 17713.
5 Q. Zhong, A. Mardyukov, E. Solel, D. Ebeling, A. Schirmeisen and P. R. Schreiner, On-Surface Synthesis and Real-Space Visualization of Aromatic P(3) N(3), *Angew. Chem., Int. Ed.*, 2023, **62**, e202310121.
6 L. Gross, F. Mohn, N. Moll, B. Schuler, A. Criado, E. N. Guitiá, D. A. Peñ, A. Gourdon and G. Meyer, Bond-Order Discrimination by Atomic Force Microscopy, *Science*, 2012, **337**, 1326.

7 D. G. de Oteyza, P. Gorman, Y.-C. Chen, S. Wickenburg, A. Riss, D. J. Mowbray, G. Etkin, Z. Pedramrazi, H.-Z. Tsai, A. Rubio, M. F. Crommie and F. R. Fischer, Direct Imaging of Covalent Bond Structure in Single-Molecule Chemical Reactions, *Science*, 2013, **340**, 1434.
8 N. Pavliček, B. Schuler, S. Collazos, N. Moll, D. Pérez, E. Guitián, G. Meyer, D. Peña and L. Gross, On-surface generation and imaging of arynes by atomic force microscopy, *Nat. Chem.*, 2015, **7**, 623.
9 F. Albrecht, N. Pavlicek, C. Herranz-Lancho, M. Ruben and J. Repp, Characterization of a Surface Reaction by Means of Atomic Force Microscopy, *J. Am. Chem. Soc.*, 2015, **137**, 7424.
10 S. Zint, D. Ebeling, T. Schloder, S. Ahles, D. Mollenhauer, H. A. Wegner and A. Schirmeisen, Imaging Successive Intermediate States of the On-Surface Ullmann Reaction on Cu(111): Role of the Metal Coordination, *ACS Nano*, 2017, **11**, 4183.
11 D. Ebeling, Q. Zhong, T. Schloder, J. Tschakert, P. Henkel, S. Ahles, L. Chi, D. Mollenhauer, H. A. Wegner and A. Schirmeisen, Adsorption Structure of Mono- and Diradicals on a Cu(111) Surface: Chemoselective Dehalogenation of 4-Bromo-3″-iodo- p-terphenyl, *ACS Nano*, 2019, **13**, 324.
12 B. Schuler, W. Liu, A. Tkatchenko, N. Moll, G. Meyer, A. Mistry, D. Fox and L. Gross, Adsorption geometry determination of single molecules by atomic force microscopy, *Phys. Rev. Lett.*, 2013, **111**, 106103.
13 S. Kawai, A. Sadeghi, T. Okamoto, C. Mitsui, R. Pawlak, T. Meier, J. Takeya, S. Goedecker and E. Meyer, Organometallic Bonding in an Ullmann-Type On-Surface Chemical Reaction Studied by High-Resolution Atomic Force Microscopy, *Small*, 2016, **12**, 5303.
14 D. Martin-Jimenez, S. Ahles, D. Mollenhauer, H. A. Wegner, A. Schirmeisen and D. Ebeling, Bond-Level Imaging of the 3D Conformation of Adsorbed Organic Molecules Using Atomic Force Microscopy with Simultaneous Tunneling Feedback, *Phys. Rev. Lett.*, 2019, **122**, 196101.
15 J. Zhang, P. Chen, B. Yuan, W. Ji, Z. Cheng and X. Qiu, Real-Space Identification of Intermolecular Bonding with Atomic Force Microscopy, *Science*, 2013, **342**, 611.
16 S. Kawai, A. Sadeghi, X. Feng, P. Lifen, R. Pawlak, T. Glatzel, A. Willand, A. Orita, J. Otera, S. Goedecker and E. Meyer, Obtaining Detailed Structural Information about Supramolecular Systems on Surfaces by Combining High-Resolution Force Microscopy with ab Initio Calculations, *ACS Nano*, 2013, **7**, 9098.
17 Z. Han, G. Czap, C.-L. Chiang, C. Xu, P. J. Wagner, X. Wei, Y. Zhang, R. Wu and W. Ho, Imaging the halogen bond in self-assembled halogenbenzenes on silver, *Science*, 2017, **358**, 206.
18 D. Ebeling, M. Sekutor, M. Stiefermann, J. Tschakert, J. E. P. Dahl, R. M. K. Carlson, A. Schirmeisen and P. R. Schreiner, London Dispersion Directs On-Surface Self-Assembly of [121]Tetramantane Molecules, *ACS Nano*, 2017, **11**, 9459.
19 J. Tschakert, Q. Zhong, D. Martin-Jimenez, J. Carracedo-Cosme, C. Romero-Muniz, P. Henkel, T. Schloder, S. Ahles, D. Mollenhauer, H. A. Wegner, P. Pou, R. Perez, A. Schirmeisen and D. Ebeling, Surface-controlled reversal of the selectivity of halogen bonds, *Nat. Commun.*, 2020, **11**, 5630.
20 J. Xu, X. Zhu, S. Tan, Y. Zhang, B. Li, Y. Tian, H. Shan, X. Cui, A. Zhao, Z. Dong, J. Yang, Y. Luo, B. Wang and J. G. Hou, Determining structural and chemical heterogeneities of surface species at the single-bond limit, *Science*, 2021, **371**, 818.
21 L. Sellies, R. Spachtholz, S. Bleher, J. Eckrich, P. Scheuerer and J. Repp, Single-molecule electron spin resonance by means of atomic force microscopy, *Nature*, 2023, **624**, 64.
22 D. Ebeling, M. Sekutor, M. Stiefermann, J. Tschakert, J. E. P. Dahl, R. M. K. Carlson, A. Schirmeisen and P. R. Schreiner, Assigning the absolute configuration of single aliphatic molecules by visual inspection, *Nat. Commun.*, 2018, **9**, 2420.
23 Q. Zhong, A. Ihle, S. Ahles, H. A. Wegner, A. Schirmeisen and D. Ebeling, Constructing covalent organic nanoarchitectures molecule by molecule via scanning probe manipulation, *Nat. Chem.*, 2021, **13**, 1133.
24 F. J. Giessibl, High-speed force sensor for force microscopy and profilometry utilizing a quartz tuning fork, *Appl. Phys. Lett.*, 1998, **73**, 3956.
25 F. J. Giessibl, The qPlus sensor, a powerful core for the atomic force microscope, *Rev. Sci. Instrum.*, 2019, **90**, 011101.
26 T. R. Albrecht, P. Grütter, D. Horne and D. Rugar, Frequency modulation detection using high-Q cantilevers for enhanced force microscope sensitivity, *J. Appl. Phys.*, 1991, **69**, 668.
27 C. Loppacher, M. Bammerlin, F. Battiston, M. Guggisberg, D. Müller, H. R. Hidber, R. Lüthi, E. Meyer and H. J. Güntherodt, Fast digital electronics for application in dynamic force microscopy using high-Q cantilevers, *Appl. Phys. A*, 1998, **66**, S215.
28 D. Martin-Jimenez, A. Ihle, S. Ahles, H. A. Wegner, A. Schirmeisen and D. Ebeling, Bond-level imaging of organic molecules using -controlled amplitude modulation atomic force microscopy, *Appl. Phys. Lett.*, 2020, **117**, 131601.
29 U. Dürig, O. Züger and A. Stalder, Interaction force detection in scanning probe microscopy: Methods and applications, *J. Appl. Phys.*, 1992, **72**, 1778.
30 R. Pawlak, S. Kawai, S. Fremy, T. Glatzel and E. Meyer, Atomic-Scale Mechanical Properties of Orientated C60 Molecules Revealed by Noncontact Atomic Force Microscopy, *ACS Nano*, 2011, **5**, 6349.
31 R. Garcia and E. T. Herruzo, The emergence of multifrequency force microscopy, *Nat. Nanotechnol.*, 2012, **7**, 217.
32 D. Ebeling, B. Eslami and S. D. Solares, Visualizing the Subsurface of Soft Matter: Simultaneous Topographical Imaging, Depth Modulation, and Compositional Mapping

with Triple Frequency Atomic Force Microscopy, *ACS Nano*, 2013, **7**, 10387.

33 D. Ebeling, Q. G. Zhong, S. Ahles, L. Chi, H. A. Wegner and A. Schirmeisen, Chemical bond imaging using higher eigenmodes of tuning fork sensors in atomic force microscopy, *Appl. Phys. Lett.*, 2017, **110**, 183102.

34 D. Martin-Jimenez, M. G. Ruppert, A. Ihle, S. Ahles, H. A. Wegner, A. Schirmeisen and D. Ebeling, Chemical bond imaging using torsional and flexural higher eigenmodes of qPlus sensors, *Nanoscale*, 2022, **14**, 5329.

35 M. G. Ruppert, D. Martin-Jimenez, Y. K. Yong, A. Ihle, A. Schirmeisen, A. J. Fleming and D. Ebeling, Experimental analysis of tip vibrations at higher eigenmodes of QPlus sensors for atomic force microscopy, *Nanotechnology*, 2022, **33**, 185503.

36 M. G. Ruppert, S. I. Moore, M. Zawierta, A. J. Fleming, G. Putrino and Y. K. Yong, Multimodal atomic force microscopy with optimized higher eigenmode sensitivity using on-chip piezoelectric actuation and sensing, *Nanotechnology*, 2019, **30**, 085503.

37 N. F. de Bem, M. G. Ruppert, A. J. Fleming and Y. K. Yong, Simultaneous tip force and displacement sensing for AFM cantilevers with on-chip actuation: Design and characterization for off-resonance tapping mode, *Sens. Actuators, A*, 2022, **338**, 113496.

38 M. Dukic, J. D. Adams and G. E. Fantner, Piezoresistive AFM cantilevers surpassing standard optical beam deflection in low noise topography imaging, *Sci. Rep.*, 2015, **5**, 1–11.

39 I. W. Rangelow, T. Ivanov, A. Ahmad, M. Kaestner, C. Lenk, I. S. Bozchalooi, F. Xia, K. Youcef-Toumi, M. Holz and A. Reum, Review Article: Active scanning probes: A versatile toolkit for fast imaging and emerging nanofabrication, *J. Vac. Sci. Technol., B:Nanotechnol. Microelectron.:Mater., Process., Meas., Phenom.*, 2017, **35**, 06G–101.

40 F. Xia, K. Youcef-Toumi, T. Sattel, E. Manske and I. W. Rangelow, Author Spotlight: Introduction to Active Probe Atomic Force Microscopy with Quattro-Parallel Cantilever Arrays, *J. Visualized Exp.*, 2023, e65210.

41 S. Sadewasser, G. Villanueva and J. A. Plaza, Special cantilever geometry for the access of higher oscillation modes in atomic force microscopy, *Appl. Phys. Lett.*, 2006, **89**(3), 033106.

42 S. I. Moore, M. G. Ruppert and Y. K. Yong, Multimodal cantilevers with novel piezoelectric layer topology for sensitivity enhancement, *Beilstein J. Nanotechnol.*, 2017, **8**, 358–371.

43 M. G. Ruppert and Y. K. Yong, Note: Guaranteed collocated multimode control of an atomic force microscope cantilever using on-chip piezoelectric actuation and sensing, *Rev. Sci. Instrum.*, 2017, **88**, 086109.

44 A. Cowen, G. Hames, K. Glukh and B. Hardy, *PiezoMUMPs Design Handbook*, MEMSCAP Inc., 2014.

45 D. C. Miller, B. L. Boyce, M. T. Dugger, T. E. Buchheit and K. Gall, Characteristics of a commercially available silicon-on-insulator MEMS material, *Sens. Actuators, A*, 2007, **138**, 130–144.

46 H. J. Butt and M. Jaschke, Calculation of thermal noise in atomic force microscopy, *Nanotechnology*, 1995, **6**, 1.

47 J. E. Sader, J. A. Sanelli, B. D. Adamson, J. P. Monty, X. Wei, S. A. Crawford, J. R. Friend, I. Marusic, P. Mulvaney and E. J. Bieske, Spring constant calibration of atomic force microscope cantilevers of arbitrary shape, *Rev. Sci. Instrum.*, 2012, **83**, 103705.

48 M. G. Ruppert, N. F. S. D. Bem, A. J. Fleming and Y. K. Yong, in *Vibration Engineering for a Sustainable Future Experiments, Materials and Signal Processing*, ed. S. Oberst, B. Halkon, J. Ji and T. Brown, Springer International Publishing, Sydney, Australia, 2021, ch. 45, vol. 2.

49 G. H. Simon, M. Heyde and H.-P. Rust, Recipes for cantilever parameter determination in dynamic force spectroscopy: spring constant and amplitude, *Nanotechnology*, 2007, **18**, 255503.

50 S. I. Moore, M. G. Ruppert and Y. K. Yong, An optimization framework for the design of piezoelectric AFM cantilevers, *Precis. Eng.*, 2019, **60**, 130–142.

51 Q. Wang, Y. Lu, S. Mishin, Y. Oshmyansky and D. A. Horsley, Design, fabrication, and characterization of scandium aluminum nitride-based piezoelectric micromachined ultrasonic transducers, *J. Microelectromech. Syst.*, 2017, **26**, 1132–1139.

52 F. Huber and F. J. Giessibl, Low noise current preamplifier for qPlus sensor deflection signal detection in atomic force microscopy at room and low temperatures, *Rev. Sci. Instrum.*, 2017, **88**(7), 073702.